Computationally determined existence and stability of transverse structures. II. Multipeaked cavity solitons

J. M. McSloy,* W. J. Firth,† G. K. Harkness, and G.-L. Oppo‡
Department of Physics, University of Strathclyde, 107 Rottenrow, Glasgow G4 ONG, Scotland
(Received 31 May 2002; published 10 October 2002)

We apply quasi-exact numerical techniques to the calculation of stationary one- and two-dimensional, bound multipeaked cavity soliton solutions of a model describing a saturable absorber in a driven optical cavity. We calculate the existence and stability domains of a wide range of such states and determine the perturbative eigenmodes that cause loss of stability. We relate the existence of *N*-peaked states to the locking range between patterned and homogeneous solutions, as a function of two parameters.

DOI: 10.1103/PhysRevE.66.046606 PACS number(s): 42.65.Tg, 42.50.Md, 42.65.Sf

I. INTRODUCTION

In the first paper [1], we presented a widely applicable Fourier-transform based, numerical technique for the determination of the existence and stability of stationary periodic patterns in a driven optical cavity containing a saturable absorber. Such solutions were characterized by their wave number and the background intensity from which they emerge, or with which they compete. We computed their domains of stability and instability. In particular, we found that hexagonal patterns may ''crack,'' breaking up into distinct islands of pattern interspersed with patches of the homogeneous solution. Such islands may contain only a few pattern elements, so that they might be considered to be clusters of solitary waves (cavity solitons) [2]. Such solitons, and their composites, are the primary topic of this second paper.

Potential applications of spatial solitons in technology are under investigation [3]. Cavity solitons are a distinct type of dissipative spatial soliton, namely individually addressable and steerable self-localized spots of light in an externally pumped optical cavity [4]. These structures have been proposed as pixel elements for an all optical memory, parallel and image processing [5–12], and for use in optical buffering [11,18]. Confinement and manipulation of small particles [13], is an interesting non-IT application. Applications interest has been heightened with the observation of cavity solitons in semiconductor microcavities. These cavity solitons have diameters of around 10 μm, evolve on and nanosecond time scales or less, and can be moved transversally at speeds in excess of 100 $\mathrm{m\,s^{-1}}$ [14,15].

Models based on a variety of nonlinear media [14,16–18] now been shown to support cavity solitons. Dissipative solitons in half cavity or feedback systems [12,20,21] have very similar properties to cavity solitons, and the term ''cavity soliton'' can be extended to imply such structures also. Experimental observations have been made in both slow [18–21] and fast [22] systems. Cavity solitons exist in a simple, but yet phenomenologically rich, model describing a saturable absorber within a driven cavity [7]. This system has also been shown to allow roll, hexagon and honeycomb patterned solutions stable over a wide range of wave vectors [1,23,24]. With the addition of Fourier feedback control, square patterns have been stablized [25].

Given this diversity of nonlinear spatial structures, it is hardly surprising that within our model there exist regions of parameter space which support both cavity solitons and higher-order solitonic structures. Multipeaked stationary states have been shown to exist in one dimension in an ac-driven nonlinear Schrödinger equation [26] and quintic Ginzburg-Landau equation [27], and there has also been a brief report of such structures in the present model (limited to one spatial dimension) [31].

In this paper, we present a detailed study of stationary multipeaked cavity soliton (CS) solutions in the above-mentioned two-level saturable absorber model (Sec. II). In Sec. III we present efficient and powerful numerical techniques to calculate these steady states and their stability. Extensive numerical analysis is performed in both a one-dimensional (1D) (Sec. IV) and the full two-dimensional (2D) model (Sec. V). We investigate such stationary structures as a function of two parameters. The stability of these solutions is calculated and respective eigenmodes determined. Finally we relate the existence domains of families of multipeaked CS to ''locking'' of fronts between the homogeneous solution and a coexistent subcritical pattern [28,29]. We track across a two-dimensional parameter space the saddle-node bifurcations at which *N*-peaked structures emerge, and compare the sequence and spacing of these bifurcations with analytical predictions [29]. We also consider, in both 1D and 2D, the ''locking range'' of individual structures, namely that in which they are stable against both expansion and shrinkage. At the former boundary, the structure invades the homogeneous background on which it sits to create an extended pattern. At the latter, it shrinks and disappears, overcome by the dominance of the homogeneous solution.

II. THE MODEL

We consider the same model as in Ref. [1], viz. an on-resonance two-level saturable absorbing medium in an externally pumped optical cavity [30]. In this model, both linear

*Electronic address: jmc@phys.strath.ac.uk
†Electronic address: willie@phys.strath.ac.uk
‡Electronic address: gianluca@phys.strath.ac.uk

and nonlinear contributions to the atomic response are real, so that the medium does not have self-focusing or defocusing properties. Conventional (propagating) spatial solitons do not, therefore exist in this medium. The spatiotemporal dynamics of the slowly varying amplitude of the electromagnetic field E is modeled by

$$\partial_t E = -E\left((1+i\theta) + \frac{2C}{1+|E|^2} \right) + E_I + i\nabla_\perp^2 E, \qquad (1)$$

where θ is the cavity mistuning of the intracavity resonance from the pump frequency, C is the scaled atomic density and so parametrizes both linear and nonlinear absorption, E_I the amplitude of the external pump field (considered a plane wave), and $\nabla_\perp^2$ is the transverse Laplacian $\partial_x^2+\partial_y^2$, which models diffraction. The time t is scaled to the cavity response time. As is evident from the denominator of the nonlinear term in Eq. (1), the field scaling is such that the saturation intensity of the transition corresponds to $|E|=1$.

As in Ref. [1], it is convenient to express Eq. (1) in terms of the deviation $[A(x,y,t)]$ from the homogeneous solution (E_0) through $E=(1+A)E_0$. We thereby obtain an equivalent equation in which solitons sit on a zero background:

$$\partial_t A = -(1+i\theta)A + \frac{2C}{1+|E_0|^2} - \frac{2C(1+A)}{1+|E_0|^2(1+A)(1+A^*)} + i\nabla_\perp^2 A. \qquad (2)$$

The intensity $|E_0|^2$ of the background field is taken to be our primary control parameter. We use, (although it has no direct physical meaning) the integral $\int |A|\, dxdy$ as a positive-definite measure with which to characterize localized solutions of Eq. (2). This measure has advantages for easy display of the complicated bifurcation structure of multipeaked cavity solitons. If, e.g., the maximum of $|A|$ is plotted, the solution branches overlie each other, as can be seen in Ref. [31].

III. NUMERICAL TECHNIQUES

Our numerical analysis of this system consists of three algorithms which we solve on a computational mesh of 128×128 gridpoints. The first directly integrates the spatiotemporal dynamics of Eq. (1) using a split-step operator integrator, in which nonlinear terms are computed via a Runge-Kutta method and the Laplacian by a fast Fourier transform (FFT) [32].

Our second algorithm is an enhanced Newton-Raphson method that can find all stable and unstable stationary solutions to Eq. (2) when $\partial A_t=0$. A Newton-FFT method has previously been used [14,17,31], for evaluation of the $\nabla_\perp^2$ operator, but solution of the resultant dense matrix is computationally intensive, especially in two spatial dimensions. To overcome this problem, here we evaluate this spatial operator using finite differences, hence obtaining a Jacobian matrix that can be inverted easily using sparse numeric library routines. As an extension to this algorithm we used an automated variable step Powell enhancement to the Newton-Raphson method [32,33], allowing it to be quasiglobally convergent, thus giving our algorithm very low sensitivity to initial conditions. All stationary, periodic or nonperiodic solutions of Eq. (2) in one and two spatial dimensions can hence be solved on millisecond and second time scales (simulations were run on SGI, Origin 300 servers with 500 MHz R14000 processors), respectively with additional speedup obtainable via OpenMP parallelization.

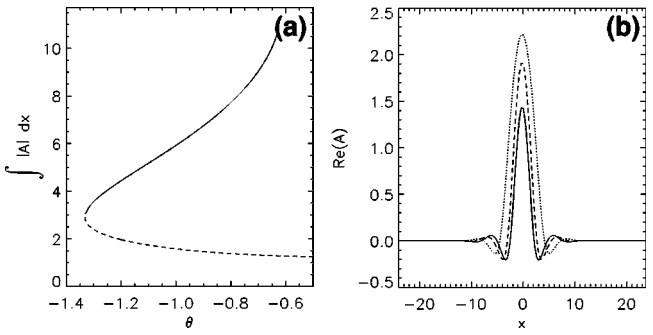

FIG. 1. (a) The integral $(\int |A|\, dx)$ of single-peaked cavity solitons versus the cavity mistuning θ; (b) Re(A) for cavity solitons on upper branch of (a): $\theta=-1.2$, solid line; $\theta=-0.92$, dashed line; $\theta=-0.63$, dotted line. $|E_0|^2=1.33$, $C=5.4$.

The third algorithm is used to determine the stability of stationary structures from our Newton algorithm. It is a sparse finite-difference algorithm based on the ''Implicitly Restarted Arnoldi Iteration'' method developed in Refs. [34,35]. We use this algorithm to solve $\hat{J}\xi=\lambda\xi$, where $\hat{J}$ is the Jacobian of derivatives of the solution in question, the roots λ are its eigenvalues and ξ the corresponding eigenmodes. This allows us to calculate the eigenspectrum in a matter of seconds/minutes (1D/2D) with approximately linear speed-up achievable across multiple processors via MPI parallelization (hardware as above). Although in this work these methods are applied to the solution of $\hat{J}$ with rank 32 768, we have used them efficiently when $\hat{J}$ has rank $\geqslant$262 144, and they could easily be modified to calculate stationary solutions and stability of *fully* three-dimensional problems.

IV. ONE-DIMENSIONAL STATIONARY STATES

To simplify our presentation and numerical analysis we work with a pump of homogeneous transverse profile. The plane-wave solution to Eq. (1) has an absorptive optical bistability (OB) threshold at $C=4$ and $\theta=0$, where $|E_0|^2=3$. Increasing $|\theta|$ increases the OB threshold. For the bulk of our studies we chose parameters close to, but outside, the OB domain so that E_0 is unique. These are $C=5.4$, $\theta=-1.2$. For these parameters the homogeneous solution exhibits a modulational instability for input field $E_I=E_{mi}=6.70$ and $|E_0|^2_{mi}=1.657$ [1]. This instability is subcritical, as is essential for the existence of stable cavity solitons. For input field $E_I=6.645$ $(|E_0|^2=1.33)$, single-peaked cavity solitons exist over a range of θ (Fig. 1). Over this range of detuning the cavity solitons are quite narrow, and well contained within the computational domain [Fig. 1(b)]. Varying

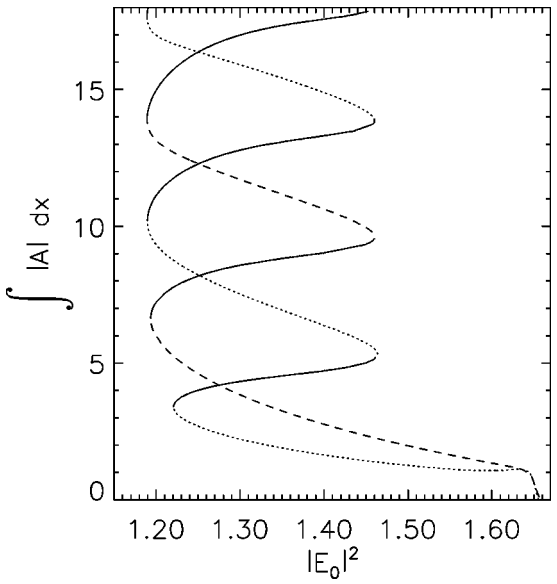

FIG. 2. Integral of one-dimensional CS structures against the intracavity field $|E_0|^2$. Solid, dotted, and dashed lines, respectively, denote: stable CS_N^{Γ}, unstable CS_{odd}^{L}, and unstable CS_{even}^{L} solutions. Parameters are $\theta=-1.2$ and $C=5.4$.

E_0 at fixed $\theta=-1.2$, it can be seen in Fig. 2 that cavity soliton branches bifurcate subcritically at the modulational instability threshold.

The existence of multipeaked CS structures is shown in Fig. 2, in which their integral ($\int |A|\ dx$) is plotted as a function of $|E_0|^2$. CS exist on two distinct yet similar branches which correspond to structures with, respectively, odd and even numbers of peaks. Both bifurcate from the homogeneous state at the point of modulational instability. Each branch, although continuous, is composed of numerous positive slope (upper) and negative slope (lower) sections, which we will denote by Γ and L superscripts, respectively. We also specify the ''number of peaks'' (N) as the number which have amplitude at least equivalent to that of the lower-branch solitary cavity soliton CS_1^L at given input parameters. A sequence of these solutions is presented in Fig. 3. Note that the N peaks are ''close packed.'' As might be guessed, there are numerous other branches corresponding to structures with at least one ''gap'' between adjacent large-amplitude peaks. If we denote such a peak by ''1,'' and a minimal ''gap'' by ''0,'' our close-packed CS structures are all of type '' . . . .00011 . . . .111000 . . . .,'' which excludes e.g. '' . . . .0001101000 . . . . .'' We will not examine such ''open structures'' in detail, although we note that their existence and stability is important in connection with the use of CS arrays as pixel or memory arrays [7,22,36].

As N increases, the solutions get broader, and so are eventually limited by the computational domain. In the absence of such constraints, they become very similar to the roll patterns described in Ref. [1]. Since a *continuum* of patterns of different wave vector are stable in this parameter region, the issue of the limiting peak separation of the multipeaked CS is an interesting question. Another issue arises when we consider that additional peaks do not have to be added symmetrically. By adding peaks on only one side one limits to '' . . . .00000111111 . . . . ,'' which is not a roll pattern, but coexistent roll and homogeneous patterns, with a *front* at the border between them. These issues will be explored below.

Turning now to the dynamical properties of these CS solutions, we have tested their stability by diagonalizing their Jacobian, using the numerical methods mentioned above. Discounting the neutral mode (see below) possessed by all CS solutions, the stability results are rather simple, in that all positive-slope branches in Fig. 2 are stable, and all negative-slope branches unstable. More precisely, all nonzero eigenvalues of the Jacobian of a positive-slope N-peak CS solution are negative, so that it is an *attractor*, self-organizing from any sufficiently-similar structure into the unique (at given parameters) CS solution on its branch.

All negative-slope CS are unstable, they in fact have only

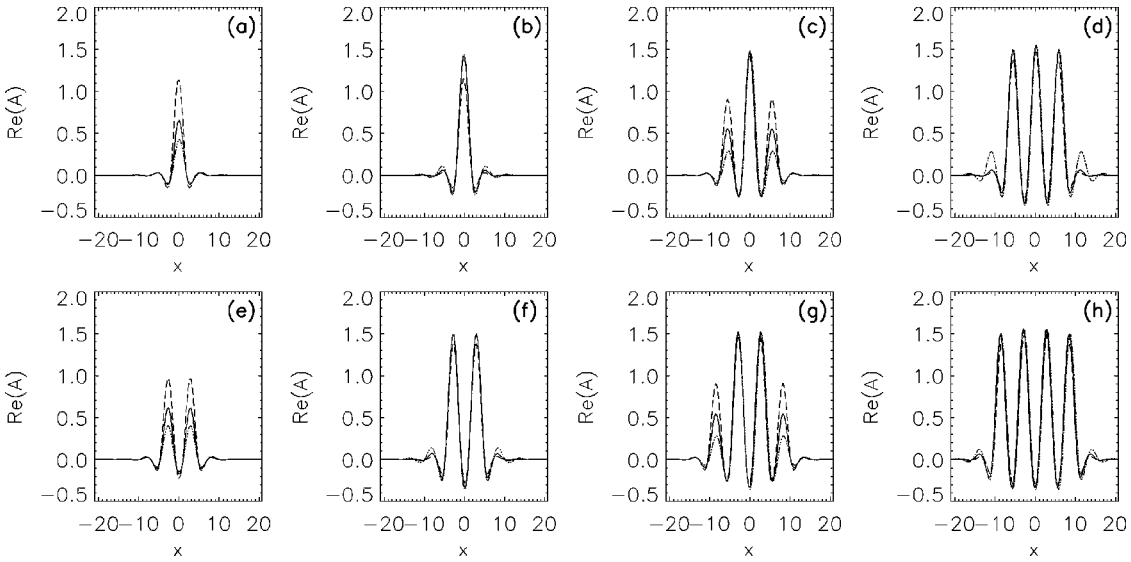

FIG. 3. Sequences of profiles for odd (left) and even (right) CS branches shown in Fig. 2. Dash-dotted, solid, and dashed lines correspond to solutions at $|E_0|^2=1.22$, $|E_0|^2=1.33$, and $|E_0|^2=1.44$. Other parameters are $\theta=-1.2$ and $C=5.4$.

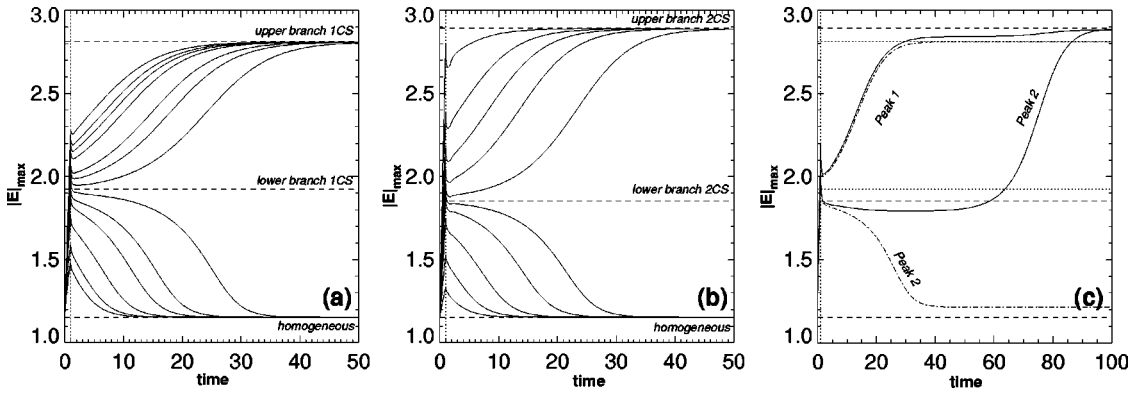

FIG. 4. Panel (a) shows the attractor nature of the lower-branch cavity soliton for CS_1 structures and panel (b) for CS_2 structures, for differing address pulses. Panel (c) gives similar behavior for (peak 1) above and (peak 2) below the separatrix. Solid and dash-dotted lines indicate two simulations in which peak 2 is ''switched on'' and where it relaxes to the side band of peak 1. The vertical dotted line denotes the address time τ. Horizontal dotted and dashed lines, respectively, show $CS_1^{\Gamma,L}$ and $CS_2^{\Gamma,L}$ structures. Parameters are $|E_0|^2=1.33$, $\theta=-1.2$, and $C=5.4$.

one positive eigenvalue, and so all their internal degrees of freedom except one are damped. Hence, as has been shown in Ref. [14], the lowest branch CS, although unstable, behaves as a *metastable* attractor for nearby states. Suppose one attempts to create a stable upper branch CS with an incident address pulse of, say, Gaussian profile for a given time τ. If the pulse is very weak, its effect will decay away and no CS will be created. Increasing the amplitude of the address pulse, one finds that the perturbation ''hump'' on the background field becomes longer lived, and also begins to resemble the lower-branch CS in shape. At this stage, the amplitude a of this hump becomes the only significant dynamical variable. If it remains less than that of the unstable CS, the hump eventually decays back into the background, and no stable CS is created as is seen below the lower-branch CS lines in Figs. 4(a) and 4(b) for an address beam suitably spaced $(2\pi/k_c)$ with dual humps of similar amplitude. If a exceeds the amplitude of the unstable CS, however, it continues to grow (even after the address pulse is over), and eventually stabilizes as a stable upper branch single-peaked CS. In the critical range, where a is very close to that of the unstable CS, the dynamics slows down dramatically, which is why we consider the unstable CS to be metastable, rather than just unstable. For higher pump values, the lower-branch amplitude decreases (Fig. 2), and it follows that the minimum energy required to excite a soliton decreases (corresponding experimentally to shorter address times or lower powers [20]). If, however, an asymmetric address pulse is applied similar to that used in Fig. 4(b) but with the second peak of amplitude slightly below the lower-branch CS, interesting results can be seen. The first peak, as expected, will grow towards the amplitude of CS_1^{Γ} structure—see Fig. 4(c). The second peak, however, relaxes below the lower-branch solutions, but due to the growth of the side bands of peaks one causes the structure to gain energy and move above the amplitude of the lower-branch CS, that eventually evolves to a CS^{Γ}. At the point of growth above the CS^{L} peak one that has been dwelling close to CS^{Γ} slowly increases in amplitude until the amplitudes of both peaks reach that of a CS_2^{Γ} structure. If, however, the peak one does not grow quickly enough the peak two will relax to the side band of peak one.

For the stable positive-slope CS_N^{Γ} structures, all internal modes are damped, and thus they usually have only one effective degree of freedom, corresponding to the neutral $(\lambda=0)$ eigenmode mentioned above. This mode, shown in Fig. 5, is associated with the transverse translational symmetry of Eq. 2. Such translational (Goldstone) CS eigenmodes are well documented [2,14,31,37]. The neutral mode, being of odd parity, couples to any local gradient of, e.g., pump field amplitude or phase present at the location of the structure. The consequent excitation of the neutral mode implies that CS move with a velocity proportional to the local gradient [7,14].

CS dynamics is more complex close to the end of a branch. We see that in one spatial dimension, lowering of $|E_0|^2$ causes a N-peaked upper branch cavity soliton CS_N^{Γ} initial condition (panels b and f) to undergo a saddle-node bifurcation to a CS_{N-2}^{L} lower-branch structure (panels a and e) when $|E_0|^2\approx 1.20$. At this saddle-node point the upper-branch structure becomes unstable to an eigenmode of form given in Fig. 6. The structure then collapses into the homogeneous background.

As the pump $|E_0|^2$ is increased, side-peaks (diffraction ripples) surrounding the main CS structure begin to grow, consistent with moving closer to the modulational instability threshold. Before this threshold is reached, however, the

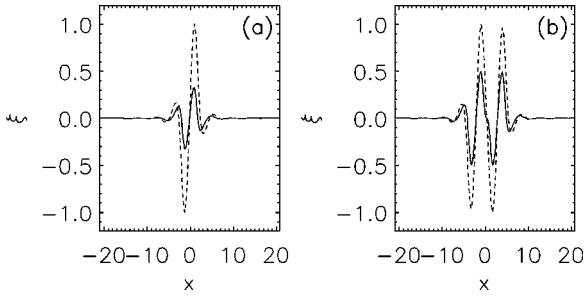

FIG. 5. Normalized neutral translational eigenmodes for CS_1^{Γ} and CS_2^{Γ} structures. Solid and dashed lines, respectively, denote $\mathrm{Re}(\xi)$ and $\mathrm{Im}(\xi)$. For both panels $|E_0|^2=1.33$.

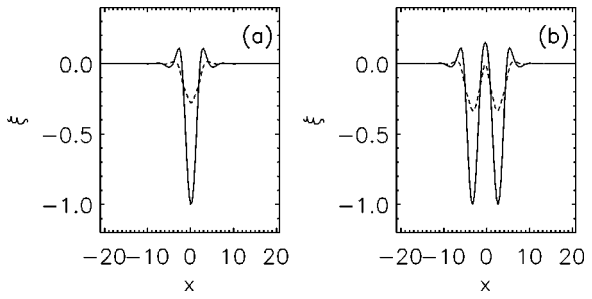

FIG. 6. Normalized unstable eigenmodes for CS_1^Γ and CS_2^Γ structures at left saddle-node bifurcation. Solid and dashed lines, respectively, denote Re(ξ) and Im(ξ). Parameters: $|E_0|^2=1.221$ (CS_1^Γ) and $|E_0|^2=1.194$ (CS_2^Γ).

strongest ripples reach a critical amplitude, where they develop a new CS peak on each side of the original structure ($|E_0|^2\approx 1.46$). This instability causes the structure to jump to an unstable CS_{N+2}^L branch (panels *c* and *g* of Fig. 3), and is a direct result of an eigenmode ξ of form shown in Fig. 7 becoming unstable at this saddle-node point, with a real eigenvalue λ becoming positive.

This instability of the side bands is a consequence of their powers exceeding that of the lower-branch soliton, which as mentioned earlier is a *separatrix* and causes growth to a full soliton. Since the newly formed higher-order soliton have identical side bands, a chain reaction occurs until a roll pattern is formed which fills the computational domain—as can be seen in Fig. 8 panel (b).

Thus we see that at one end of a CS branch, pattern dominates over background, whereas at the other the background dominates as the CS solutions collapse. Pomeau [28] considered the dynamics of the front between a roll pattern and the coexistent homogeneous solution (symbolized by "....00000111111...." in the Introduction). He showed that this front generically moves, i.e., there is a more stable phase that annihilates the less stable one, but that there can be an intermediate region in which the two phases can stably coexist over a finite range of a given parameter. In this region the front "locks" and remains stationary. Our *N*-peaked CS solutions can be symbolized as "....00011111....111110000....," which we can envisage as a pair of fronts "back-to-back." This idea has been

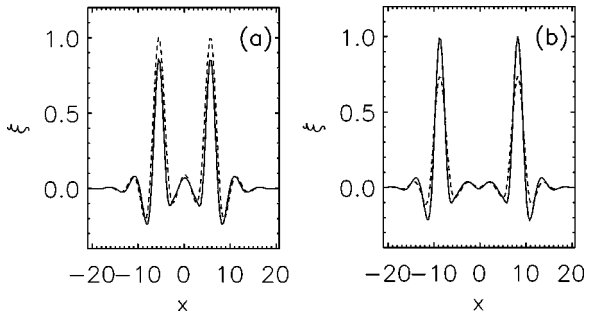

FIG. 7. Normalized unstable eigenmodes for CS_1^Γ and CS_2^Γ structures at right saddle-node bifurcation. Solid and dashed lines, respectively, denote Re(ξ) and Im(ξ). Parameters: $|E_0|^2=1.464$ (CS_1^Γ) and $|E_0|^2=1.447$ (CS_2^Γ).

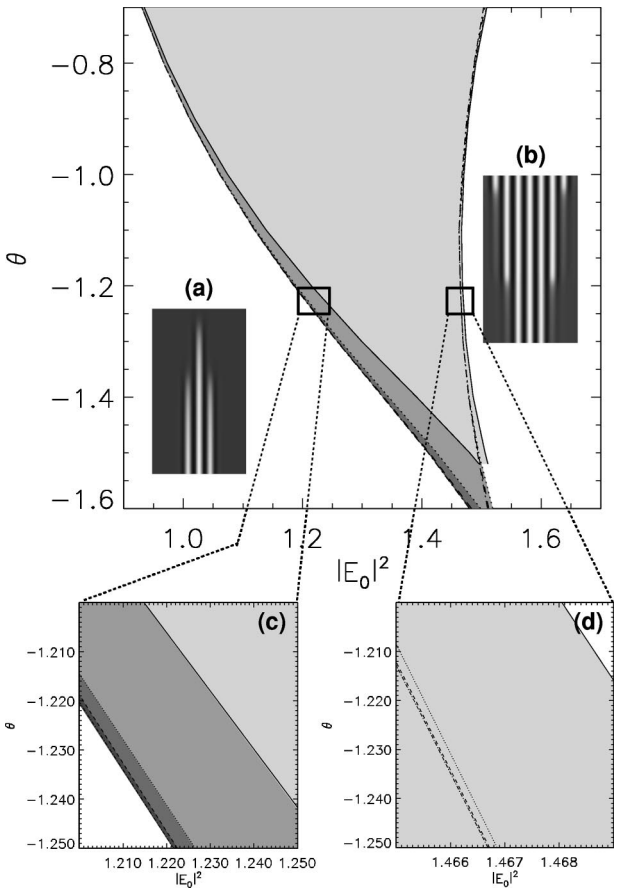

FIG. 8. Regions of existence limits 1D CS_N^Γ structures (shaded regions) in two-dimensional parameter space ($|E_0|^2,\theta$). Structures with $N=1$, 2, 3, and 4, respectively, exist between solid, dotted, dashed, and dash-dotted lines. Panels (a) and (b) show space-time plots of unlocking behavior, with the transverse coordinate *x* on the horizontal axis and time *t* increasing on the vertical axis. Panel (c) shows the fine structure of locking domain, indicated by the square on the main figure. Parameters: $C=5.4$.

given an analytical justification by Coullet *et al.* [29]. Within the regions of stability of CS_N^Γ structures we can thus talk of *locking* in analogy with these analytical results [28,29]. From the saddle-node bifurcations in Fig. 2 it is clear (and fortunate from an applicational viewpoint) that high-order clusters of cavity solitons can be stable over a finite range of $|E_0|^2$. Knowing the existence and stability properties of CS solutions as functions of $|E_0|^2$ for fixed θ and *C*, we can add a second dimension in parameter space, extending Fig. 2, along θ in the ($|E_0|^2,\theta$) plane, as shown in Fig. 8 for $CS_{1,2,3,4}^{\Gamma,L}$ structures. At the boundaries of these regions, unlocking takes place due to the invasion of the homogeneous solution into a patterned state or pattern into a homogeneous state [see, panels (a) and (b) in Fig. 8]. The fine structure of such locking domains is shown in panel (c).

These solutions have stable and unstable multisectioned branches which connect through saddle-node bifurcations. By analyzing these sections ($CS_{1,2,3,4}^\Gamma$) with θ fixed, the value of $|E_0|^2$ for each CS_N^Γ structure at each saddle-node bifurcation point (which we term μ_N) is determined. The values of

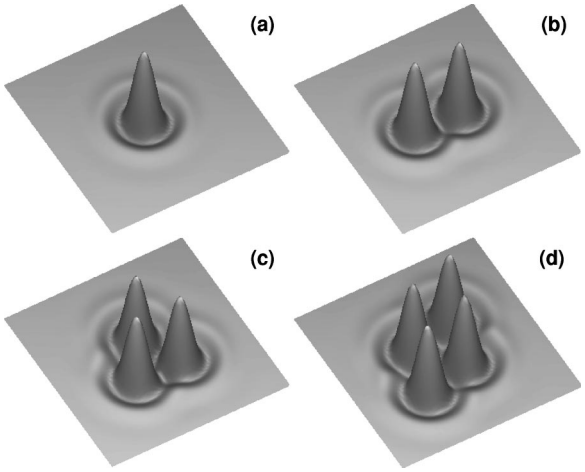

FIG. 9. Stable $CS^{\Gamma}_{1,2,3,4}$ clusters found using our Newton algorithm in a physical domain of 48×48 diffraction lengths on a computational mesh of 128×128 grid points. Parameters: $|E_0|^2=1.33$, $\theta=-1.2$, and $C=5.4$.

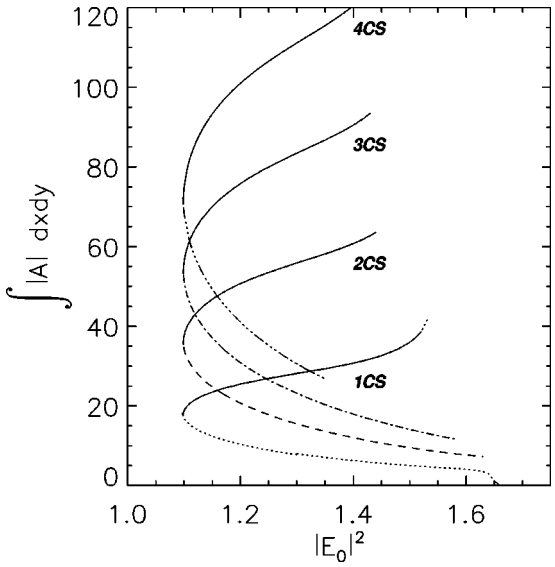

FIG. 10. Integral of two-dimensional CS structures against the external pump $|E_0|^2$. Respectively denoted for ascending integral values are solid CS^{Γ}_N and broken CS^{L}_N lines, where $N=1,2,3,4$. Parameters: $\theta=-1.2$ and $C=5.4$.

μ_N should obey a similar scaling principle to that presented in Ref. [29] for localized structures in the Swift-Hohenberg equation. For large N this scaling is predicted to be geometric, i.e. given by

$$\mu_{N+1}-\mu_N=r(\mu_N-\mu_{N-1}), \tag{3}$$

where r is a constant. We can try to test this prediction, over a two-dimensional parameter space, against the data from our model presented in Fig. 8. We can report that the sequence of bifurcations is precisely as predicted in Ref. [29], and moreover, that this sequence is maintained along any section of the CS domain in Fig. 8. We cannot confirm the geometric scaling law, however, but cannot yet say whether this is due to imprecision in our numerical data, to not having reached the asymptotic region of N, or indeed to the scaling law being invalid.

Fig. 8 shows the existence of a particularly interesting region in 1D parameter subspace, where $|E_0|^2\approx1.49$. At these parameters we obtain two separate ranges of θ in which cavity solitons exist.

V. TWO-DIMENSIONAL STATIONARY STATES

Multipeaked cavity soliton structures in two dimensions involve 2D interaction forces between neighboring solitons. This feature has been studied recently in Ref. [2], where the stability of two-dimensional clusters of cavity solitons was analyzed as a function of soliton separation. Stable separations are determined by an effective potential created by the interaction of the diffraction ripples of the N cavity solitons, which was found to be expressible as a sum of pair-wise potentials within the structure. In Ref. [2] the emphasis was primarily on open clusters, because the interaction potential is only asymptotically exact. Here, in a numerical analysis, we only consider close-packed clusters, at the first stable separation distance of $d\approx6.8$ for CS^{Γ}_N configurations, as shown in Fig. 9. It should be noted that for CS^{Γ}_4, square configurations of side d are unstable due to diagonal interactions [see, Ref. [2]], and so for $N=4$ we consider the rhomboid of side d, which is stable.

Figure 10 shows the integral measure of the 2D CS solutions with $N=1,2,3,4$ close-packed peaks. There is a strong qualitative similarity to the corresponding 1D plot (Fig. 2), but it should be noted that there is no known scaling law for 2D structures to match that for 1D [29]. In this two-dimensional model, the existence and stability domains of multipeaked cavity solitons in the $(|E_0|^2,\theta)$ parameter space are also quite similar to those found in our one-dimensional analysis, and so we present only those for CS^{Γ}_1, CS^{Γ}_2, CS^{Γ}_3 and CS^{Γ}_7 structures. These are shown in Fig. 11, again with their existence domains extended. These stability domains are important because of cavity mistuning and pumping inhomogeneities present in experimental nonlinear media, that make it desirable to have large domains of stability. While the structure of the overlaid domains in Fig. 11, are qualitatively similar to the 1D case, we again note that there is no analytic law with which to compare the bifurcation sequences.

Panels (a) and (b) of Fig. 11, respectively, show 3D space-time plots of unlocking behavior, with the transverse coordinates (x,y) on the vertical axis and time t on the horizontal axis. In panel (a) a CS^{Γ}_7 becomes unstable to the invasion of the homogeneous solution into the structure, while in panel (b) the opposite is true and the structure invades the homogenous solution forming an extended optical pattern.

Mechanisms responsible for these unlocking characteristics are of obvious importance. Starting from a solitary CS^{L}_1 structure we find that decreasing the pump has the effect of weakening the diffraction ripples surrounding the soliton. At the lower existence threshold ($|E_0|^2\approx1.10$) the structure becomes unstable to an undamped eigenmode which causes the CS^{Γ}_1 structure to eventually relax into the homogenous state.

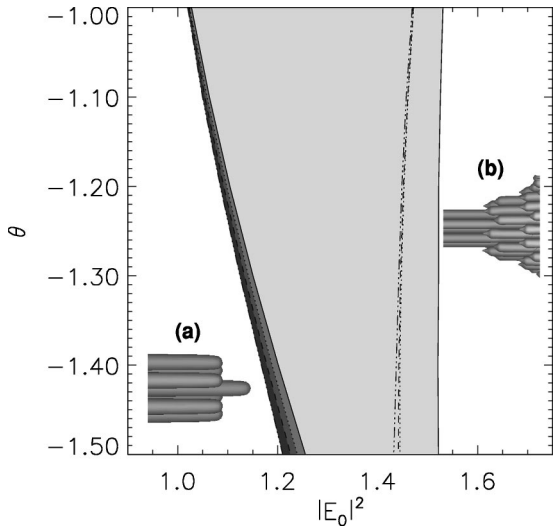

FIG. 11. Locking regimes of hexagonal clusters of CS_1^Γ (solid/light gray), CS_2^Γ (dotted/gray), CS_3^Γ (dashed/dark gray), and CS_7^Γ (dot-dashed/black) structures, with respective existence indicated by (line style/fill shade). Panels (a) and (b) show the unlocking dynamics of a CS_7^Γ structure at amplitude $|E|=1.5$, with transverse coordinates (x,y) on the vertical axis and time t increasing on the horizontal axis. Respective intracavity field intensities are $|E_0|^2=1.08$ and 1.45 with $\theta=-1.2$ and $C=5.4$.

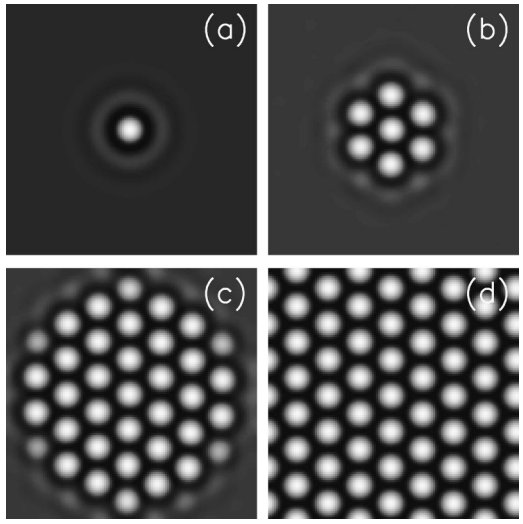

FIG. 13. Dynamical evolution of CS_1^Γ structure at $|E_0|^2_{max}$. Panels (a)–(d), respectively, give the field E at $t=0$, $t=45$, $t=80$, and $t=400$. Parameters: $|E_0|^2=1.5326$, $\theta=-1.2$, and $C=5.4$.

As in the 1D case, increasing the pump generates stronger diffraction ripples around the structures. If the pump is increased to the upper existence threshold ($|E_0|^2\approx 1.52$) the primary ring splitsup into a periodically disturbed annulus. Unlike the one-dimensional analysis though, there are four competing eigenmodes which become undamped at this point (see Fig. 12). These lead to the formation of six, four, five, and seven modulated peaks around the primary diffraction ring, as shown in panels (d)–(g), respectively. The mode with six-fold symmetry [panel (d)] is the dominant one, and subsequently causes a bifurcation to an unstable CS_{N+6}^L solution. This then evolves towards a hexagonal patterned state as seen in Fig. 13, thus verifying the picture given in Fig. 11 panel (b). At the end of the existence branch ($|E_0|^2=1.5326$) an $m=0$ eigenmode becomes undamped as predicted in Ref. [7].

VI. CONCLUSIONS

We have applied powerful numerical techniques to efficiently calculate one- and two-dimensional steady-state cavity soliton solutions, and their stability. We demonstrated these techniques in the context of a simple but rich nonlinear optics model, but they have wide applicability. These structures have been shown to exist in substantial regions of a two-dimensional parameter space, in separate branches which bifurcate from the homogeneous background solution. The stability and dynamics of the solutions on each branch have been studied, and we have characterized their eigen-

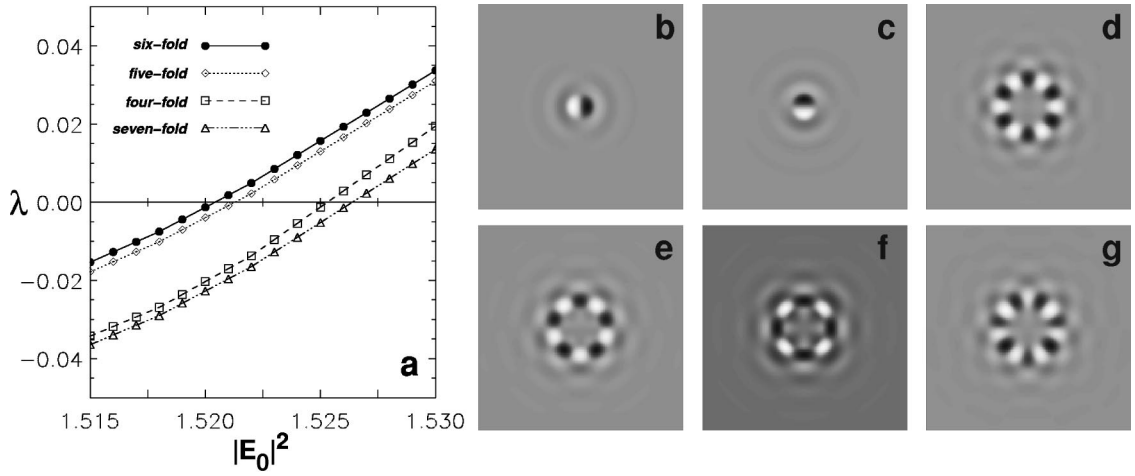

FIG. 12. Eigenmodes plotted as a function of $|E_0|^2$ for CS_1^Γ structure. Respective eigenvalues for panels (b)–(g) are $\lambda=0$, 0, 3.7×10^{-2}, 3.5×10^{-2}, 1.7×10^{-2}, 1.5×10^{-2}. Parameters: $|E_0|^2=1.53$, $\theta=-1.2$, and $C=5.4$.

modes. We have identified the modes which become undamped at the saddle-node bifurcation marking the end of each branch (or subbranch). We have also found the spatial modes responsible for the formation of higher order solutions. Finally we identified the overlaid domains in which one- and two-dimensional structures exist as stable ''locked'' solutions in a two-parameter space. In one dimension, the sequence of bifurcations at the boundaries of these domains is in general agreement with an asymptotic analytic prediction. We obtained and discussed the corresponding sequences in two dimensions, for which no analytic formulas are known.

ACKNOWLEDGMENTS

This research was partially supported by EPSRC Grant Nos. GR/M 31880, GR/M 19727, GR/N 19830, and GR/R 04096, ESPRIT Project No. 28235, PIANOS [11] and QUANTIM (Grant No. IST-2000-26019). G.-L.O. acknowledges support from SGI. We thank A. J. Scroggie for illuminating discussions relating to this paper.

[1] G.K. Harkness, W.J. Firth, G.-L. Oppo, and J.M. McSloy, Phys. Rev. A **66**, 046605 (2002).
[2] A.G. Vladimirov, J.M. McSloy, D.V. Skryabin, and W.J. Firth, Phys. Rev. E **65**, 046606 (2002).
[3] G.I.A. Stegman, D.N. Christodoulides, and M. Segev, IEEE J. Sel. Top. Quantum Electron. **6**, 1419 (2000).
[4] W.J. Firth, *Soliton-Driven Photonics*, edited by A.D. Boardman and A. P. Sukhorukov (Kluwer Academic Publishers, London, 2001), pp. 459–485.
[5] G.S. McDonald and W.J. Firth, J. Opt. Soc. Am. B **7**, 1328 (1990).
[6] A.N. Rakhmanov, Opt. Spektrosk. **74**, 701 (1993).
[7] W.J. Firth and A.J. Scroggie, Phys. Rev. Lett. **76**, 1623 (1996).
[8] W.J. Firth, A. Lord, and A.J. Scroggie, Phys. Scr., **T67**, 12 (1996).
[9] N.N. Rosanov, Prog. Opt. **35**, 1 (1996); see, also, N.N. Rosanov, *Spatial Hysteresis and Optical Patterns* (Springer-Verlag, Heidelberg, 2002).
[10] L. Spinelli, G. Tissoni, M. Brambilla, F. Prati, and L. Lugiato, Phys. Rev. A **58**, 2542 (1998).
[11] Processing of Information by Arrays of Nonlinear Optical Solitons homepage, www.pianos-int.org
[12] B.A. Samson and M.A. Vorontsov, Phys. Rev. A **56**, 1621 (1997).
[13] A.J. Scroggie, G.-L. Oppo, and W.J. Firth, *Optical Sprinklers* (CLEO/Europe-IQEC, 2000).
[14] T. Maggipinto, M. Brambilla, G.K. Harkness, and W.J. Firth, Phys. Rev. E **62**, 8726 (2000).
[15] A.J. Scroggie, J.M. McSloy, and W.J. Firth, Phys. Rev. E **66**, 036607 (2002).
[16] L.A. Lugiato and R. Lefever, Phys. Rev. Lett. **58**, 2209 (1987).
[17] G.-L. Oppo, A.J. Scroggie, and W.J. Firth, Phys. Rev. E **63**, 066209 (2001).
[18] W.J. Firth and C.O. Weiss, Opt. Photonics News **26**, 54 (2002).
[19] A.N. Rakhmanov and V.I. Shmalhausen, Proc. SPIE **2108**, 428 (1993).
[20] A. Schreiber, B. Thüring, M. Kreuzer, and T. Tschudi, Opt. Commun. **136**, 415 (1997).
[21] B. Schäpers, M. Feldmann, T. Ackemann, and W. Lange, Phys. Rev. Lett. **85**, 748 (2000).
[22] V.B. Taranenko, C.O. Weiss, and B. Schäpers, Phys. Rev. A **65**, 013812 (2001).
[23] W.J. Firth and A.J. Scroggie, Europhys. Lett. **26**, 521 (1994).
[24] G.K. Harkness, W.J. Firth, and G.-L. Oppo, in Proceedings of International Quantum Electronic Conference, Nice, 2000.
[25] R. Martin, A.J. Scroggie, G.-L. Oppo, and W.J. Firth, Phys. Rev. Lett. **77**, 4007 (1996).
[26] I.V. Barashenkov, Yu.S. Smirnov, and N.V. Alexeeva, Phys. Rev. E **57**, 2350 (1998).
[27] J.M. Soto-Crespo, N. Akhmediev, and K.S. Chiang, Phys. Lett. A **291**, 115 (2001).
[28] Y. Pomeau, Physica D **23**, 3 (1986).
[29] P. Coullet, C. Riera, and C. Tresser, Phys. Rev. Lett. **84**, 3069 (2000).
[30] L.A. Lugiato and C. Oldano, Phys. Rev. A **37**, 3896 (1988).
[31] W.J. Firth and G.K. Harkness, Asian J. Phys. **7**, 665 (1998).
[32] W.H. Press, S.A. Teukolsky, W.T. Vetterling, and B.P. Flannery, *Numerical Recipes—The Art of Scientific Computing*, 2nd ed. (Cambridge University Press, Cambridge, 1993).
[33] N. Köckler, *Numerical Methods and Scientific Computing* (Oxford University Press, Oxford, 1994).
[34] ARPACK–Arnoldi Package, www.caam.rice.edu/software/ARPACK
[35] R.B. Lehoucq, D.C. Sorensen, and C. Yang, *Solutions of Large Scale Eigenvalue Problems with Implicitly Restarted Arnoldi Methods* (Rice University, Houston, 1997).
[36] W.J. Firth (unpublished).
[37] S. Longhi, Phys. Rev. E **55**, 1060 (1997).